DOI: 10.22226/2410-3535-2017-4-428-432 PACS: 62.20.mm, 62.20.fq

Plastic and fracture behaviour of nanocrystalline binary Al alloys with grain boundary segregation

R. I. Babicheva[1,2,†], S. V. Dmitriev[2], V. V. Stolyarov[3], K. Zhou[1]

[†]ri.babicheva@gmail.com

[1]Nanyang Technological University, 50 Nanyang Ave., Singapore, 639798, Singapore
[2]Institute for Metals Superplasticity Problems of RAS, 39 Khalturin St., Ufa, 450001, Russia
[3]Mechanical Engineering Research Institute of RAS, 4 Maly Kharitonyevsky Pereulok, Moscow, 101990, Russia

The paper studies the stress-strain and fracture behaviour of nanocrystalline (NC) pure Al and NC binary Al-X alloys (X can be Fe, Co, Ti, Mg or Pb) with grain boundary (GB) segregation during their tensile deformation at room temperature via molecular dynamics simulation. The computational cell used for the modeling contains nano-sized grains of Al majority of which has the high-angle type GBs. The binary alloys were obtained through the substitution of Al atoms in GBs by atoms of the alloying elements. Stress-strain curves of the considered materials were calculated, and their microstructure evolution was analyzed. It was found that GB segregations can significantly alter the deformation behaviour of NC Al. The NC pure Al and two alloys, Al with Fe and Al with Mg, undergo the intergranular fracture which is noticeable already at ~8% strain, while the other alloys do not demonstrate any failure process up to 40% deformation. The main crack growth mechanism is the formation of nano-voids at GBs and triple junctions followed by their coalescence at higher applied stresses. The obtained results demonstrate that GB segregation of Co can have a positive effect on both plasticity and strength of NC Al, and Ti atoms in GBs can result in its improved ductility.

Keywords: molecular dynamics; nanocrystalline aluminium; fracture; grain boundary segregation.

1. Introduction

Nanomaterials, such as nanofilms and nanowires, as well as bulk nanocrystalline (NC) metallic materials which demonstrate high strength, damage resistance and unique functional properties have been receiving increased interest [1 – 13] and always are in demand of various applications. Obviously, along with a chemical composition, the macroscopic properties of such materials are mostly determined and dictated by the microstructure features. Therefore nowadays, there is a burst of interest towards modifying the structure of materials, for example, grain size and grain boundary (GB) structure, in order to enhance their properties.

Reducing an average grain size of polycrystalline materials to the nanoscale level by using severe plastic deformation, rapid solidification or crystallisation of amorphous phase allows noticeably increasing their strength and enhancing functional properties. The GB strengthening mechanism observed in fine-grained structure materials can be associated with three main factors: 1) the dislocation pile-up resulting in a stress concentration [14,15]; 2) the active dislocation interaction due to the decrease in the mean free path and therefore, the increase in the work-hardening rate [16]; 3) the contribution of GBs as sources of dislocations [17]. At the same time, fine-grained materials demonstrate strength much higher than could be expected only from the Hall-Petch relationship. Evidently that such behaviour cannot be explained only by the grain size strengthening and involves mechanisms related to GB structure [18]. The unique properties of NC materials can be also associated with such deformation mechanisms as grain boundary sliding (GBS), GB diffusion-controlled creep and triple line diffusion [19].

Another important factor controlling mechanical properties of NC materials is GB segregation. GB segregation engineering (GBSE) implies manipulation and transformation of GBs via solute decoration for improvement of material properties [20]. GBSE is mainly based on the ability of GB segregations to increase GB cohesion and strength of materials [21 – 26], stabilize NC grains by inhibiting GB motion (GBM) [27 – 29]. In addition, they can improve damage resistance and promote local phase transformation [30,31] that can make materials more resistant against crack penetration and initiate a nanoscale plasticity [32,33]. It was shown that the ability of GB segregations to change deformation mechanisms can lead to improved fatigue characteristics of NC materials [34].

Despite a growing number of works on GBSE, only some common rules for different materials are available so far, that is insufficient for the full understanding of the GB segregation effect on the mechanical behaviour of NC materials and their widespread application. It can be attributed to the fact that the GB segregation is an atomic scale phenomenon, and therefore precise data characterizing structure and chemistry of GBs are often hard to obtain experimentally. In this case, impossible, dangerous and costly experiments can be replaced by molecular dynamics (MD) simulation. Given this, the aim of the present work is to study plastic and fracture behaviour of NC Al with GB segregation using MD simulation.

2. Modeling

2.1. Materials of study

The MD simulation is performed for NC Al constructed in a three-dimensional cuboidal computational cell using the Voronoi procedure. The cell contains about 100 randomly oriented nano-sized crystals or grains of Al (Fig. 1.) The average size of the grains is ~10 nm. The cell has the edge length of 42 nm and contains almost 5 million atoms. Commonly, atoms in Al GBs have a coordination number different from 12 of the ideal fcc lattice. To create a structure with segregation in GBs, Al atoms with the coordination number equal to 11 or 10 are replaced by a type of alloying atoms, which can be Fe, Co, Ti, Mg or Pb. This procedure results in the alloying element concentration of 10.2%, as averaged over the whole computational cell.

2.2. Simulation setup

It is believed that the embedded-atom method (EAM) potentials [35] are perhaps one of the most appropriate types of interatomic potentials for MD simulation of metallic systems. Therefore in the current work, the interatomic forces are described by the many-body EAM potentials. Overall, the EAM interatomic potentials used for the simulation can reproduce elastic and plastic properties of the pure Al and the studied binary systems quite well [36 – 41]. In particular, potentials for the studied systems were taken from the following works: Al [36], Al-Mg [37], Al-Fe [38], Al-Ti [39], Al-Pb [40], Al-Co [41]. At the same time, there are some shortcomings in these potentials that should be mentioned. For example, the fact that the potential for Al-Mg [37] reproduces the liquidus and solidus lines fairly well yet somewhat underestimates the liquid enthalpy of mixing, suggests that there is some discrepancy in the description of the mixing entropy. As for the Al-Ti system, the fit to elastic constants is better than with previous potentials but it is not as good as that for Al [39]. In the case of the Al-Co potential [41], there is some insignificant discrepancy in the formation energy of B2 AlCo. It is lower by 0.07 eV/atom compared to experiment. Experimental solubility limits for the Al-Pb system are higher, especially on the Al-rich side, than those calculated by means of the potential used in the study [40]. The main drawback of the Al-Fe interatomic potential mentioned in the source is that the simulation results performed with a Fe concentration of 8 ppm show the overestimated activation energy for GBM [38].

The simulation is conducted by LAMMPS program package [42]. For visualization of a structure, the open source OVITO software is adopted [43]. The periodic boundary conditions are applied along the three orthogonal directions of the computational cell.

The NC Al and its alloys are relaxed at zero temperature to obtain the state of the minimum potential energy. Then, the cell is equilibrated for 50 ps at the corresponding deformation temperature. The NPT ensemble (constant number of atoms, pressure and temperature) is employed for the modeling of tensile deformation with the constant strain rate of 10^8 s^{-1}. A uniaxial tensile loading is applied to the NC materials at 300 K up to 40% deformation. All the stress components except σ_{xx} are fixed to be zero.

3. Results

3.1. Stress-strain curves

Fig. 2 shows stress-strain curves for the NC pure Al and its binary alloys with GB segregation of Fe, Co, Ti, Mg and Pb obtained during the tension at 300 K. It is seen from the curves that three materials, namely the pure Al and the Al-Mg and Al-Fe alloys, undergo fracture, while the other alloys do not demonstrate a failure up to the 40% deformation.

For all the considered materials, the strength is higher than that at the shear loading. The GB segregation of Co or Fe noticeably enhances the Al strength, while Pb leads to the opposite effect and decreases ultimate stresses of Al from 1.80 to 1.15 GPa. The Ti and Mg atoms in GBs slightly decrease the strength of Al. The addition of Co or Fe strengthens Al from 1.80 to 2.27 and 2.20 GPa, respectively. After reaching the yield point, stresses of the Al alloys with Co and Ti drop down to the stable plastic flow level at ~1.8 and 1.4 GPa, respectively, and with the further deformation, almost do not undergo any changes. For the Al-Pb alloy, stresses increase gradually, reach the saturated level of the ultimate strength and then, similar to the alloys with Co and Ti, do not demonstrate any significant changes up to the 40%

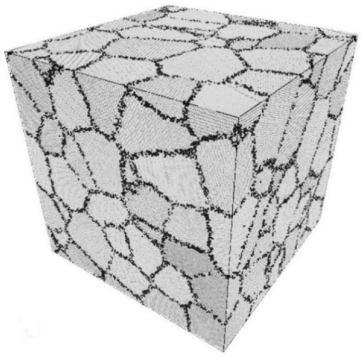

Fig. 1. MD computational cell of Al with GB segregation of alloying element (in black).

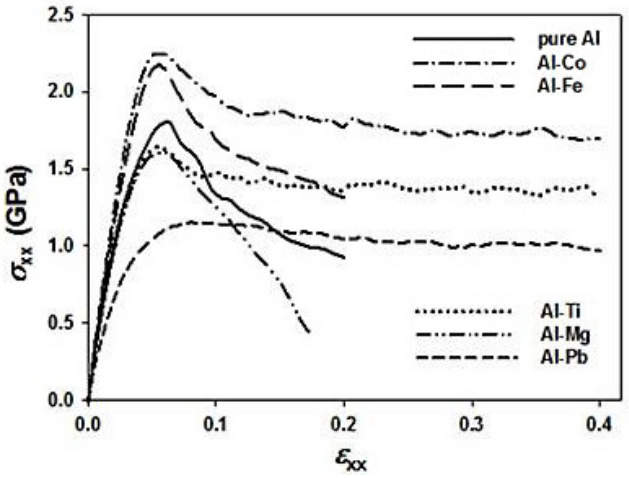

Fig. 2. Stress-strain curves of the NC pure Al and its binary alloys with GB segregation.

deformation. As a result of fracture process, the stresses of the other considered materials (pure Al, Al-Mg and Al-Fe) decrease sharply right after reaching the ultimate strength at ~5% tensile deformation. Since within the studied materials only the pure Al and the Al-Mg and Al-Fe alloys undergo failure, further, the fracture analysis is carried out only for these three materials.

3.2. Fracture

In Fig. 3, an evolution of the NC pure Al structure during the uniaxial tension at room temperature is demonstrated. In order to make GBs more visible, the results of the common neighbour analysis (CNA) is given in the figure. Here, atoms of the fcc, hcp and disordered structure are shown in green, red and gray colors, respectively, while cracks forming during the deformation are given in black. A corresponding deformation level is indicated over each snapshot. First micro-voids or cracks can be seen already at ~8% deformation. Obviously that the cracking process is accompanied by the decrease in stresses (see Fig. 2). The first micro-voids nucleate preferably at triple junctions of GBs or close to them in GBs and then propagate perpendicular to the direction of loading along GBs.

The fracture process in the Al-Mg alloy is presented in Fig. 4. Here, the upper row of snapshots is given to demonstrate a location of Al (in light blue) and Mg atoms (in dark blue), while in the lower snapshots, similar to the pure Al case, CNA pictures are shown. First voids are noticeable at ~6% deformation. Similar to the pure Al, the Al-Mg alloy demonstrates the intergranular fracture upon deformation. The fracture process is accompanied with formation of multiple micro-voids in GBs and further their coalescence. Such process of crack growth has been well described earlier in the literature devoted to the study of fatigue crack growth mechanisms [44 – 46].

Fig. 5 represents the cracking process in the NC Al alloy with GB segregation of Fe. Similar to the previous figures, the atomic structure with Al (in light blue) and Fe atoms (in dark blue) is given in the upper row of snapshots, while in the lower snapshots, the CNA pictures are shown.

The failure occurs via the intergranular fracture that is clearly seen from the CNA snapshots; cracks propagate inside a disordered structure of GBs, though from the upper snapshots, one can observe that the cracks are away from the Fe atoms. At the same time, for the Al-Mg alloy, the cracks propagate as if they split the layer of the segregated atoms in GBs into two parts (Fig. 4). Apparently, such difference can be explained by the fact that Fe has the weaker drag force compared to Mg that results in some GBM from the segregation of Fe atoms. This leads to some weakening of GBs and their separation which accompanied with the break of Al-Al interatomic bonds. In the case of the Al-Mg alloy, GBs do not migrate but, apparently, the Al-Al and Al-Mg bonds are stronger than the Mg-Mg bonds, and therefore GBs easily cleavage. These results are in a good agreement with the calculation of the embrittlement potency and the GB segregation energy of the considered alloying elements in GB of Al reported in our previous work [25]. The obtained GB segregation energy and the embrittlement potency for Mg and Fe in GBs showed that generally, Mg does not strengthen GBs, while due to the weak drag force, Fe does not stay in GBs, and therefore no GB strengthening effect can be expected for this element. It is revealed that in the Al-Mg alloy, the cracking process starts earlier and more intensive compared to the pure Al and Al-Fe alloy. The directions of crack growth in both the alloys are similar to that observed for the pure Al.

4. Discussion

The stress-strain behaviour of the materials is defined by acting deformation mechanisms. The structure analysis suggests that the dislocation sliding makes a small contribution to the deformation of the NC Al and its alloys. This statement is in agreement with a number of studies which prove that plastic deformation of NC materials is not dominated by the dislocation slip, especially at room

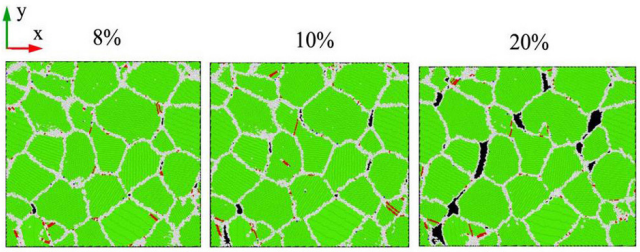

Fig. 3. (Color online) Fracture of the NC pure Al.

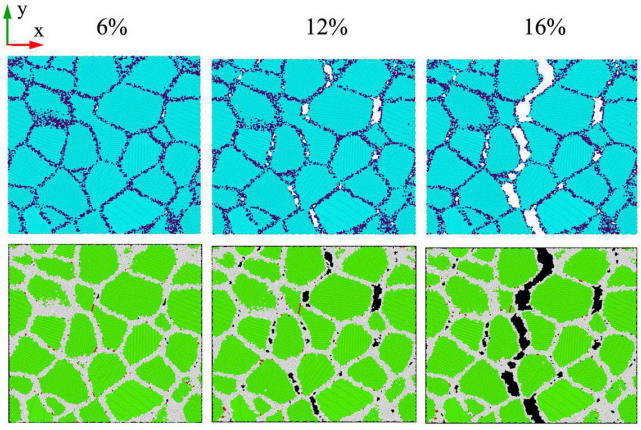

Fig. 4. (Color online) Fracture of the NC Al with GB segregation of Mg.

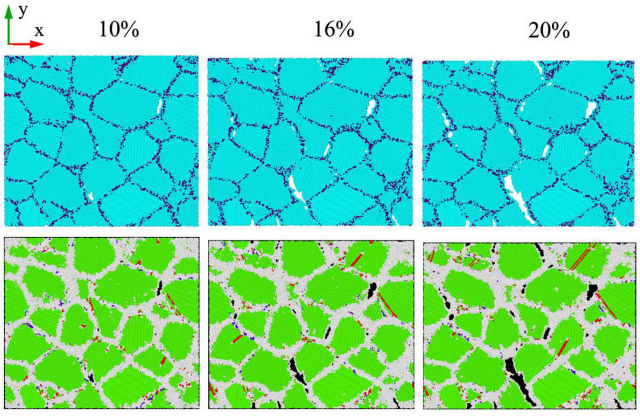

Fig. 5. (Color online) Fracture of the NC Al with GB segregation of Fe.

temperature [47 – 49]. GBS and GBM play an important role during plastic deformation of NC materials. Thus, it was revealed earlier that the deformation of the NC pure Al is associated with the shear-coupled migration of GBs that leads to the decrease of material strength [28].

GB segregations can significantly alter the deformation mechanisms. For example, within the considered systems, the NC alloy with Co atoms in GBs is the best material in term of strength and ductility. The high strength of the material can be explained by the ability of the Co GB segregation to retard GBM and GBS that was shown in [28]. There exists a number of works that prove the positive effect of Co on mechanical properties of Al alloys. For example, it has been observed that Al-Co alloys obtained by the melt spinning technique have high strength and ductility [50], while an improvement in the thermal stability and corrosion resistance of the ternary amorphous Al-Ni-Y alloys after the Co addition has been demonstrated in [51]. It is known that Co atoms can easily lead to amorphisation of GB regions [28] that can inhibit the intergranular fracture and increase the ductility of alloys. This process is close to the transformation-induced nano-scale plasticity that can prevent the void formation [32,33].

GB segregation can also affect the cracking process in NC Al. Thus, Mg weakens GBs promoting cracking, and Fe does not stay in GBs during deformation [25], and therefore the Al-Fe alloy behaves close to the pure Al. In addition, alloying elements which atomic sizes differ significantly from that of Al, such as Mg and Fe, can create high stress concentrations around them that promote void formation along GBs. Moreover, as was mentioned earlier, during deformation, GB segregation can influence GBS and accommodation mechanisms that characterize plastic deformation of grains without void nucleation [52].

5. Conclusions

The MD simulation was conducted to investigate the deformation and fracture behaviour of the NC binary Al alloys with GB segregation. The results were compared to those for the NC pure Al.

The tensile loading of the NC binary Al alloys with GB segregation of Co, Ti or Pb does not lead to any crack formation up to 40% deformation, while the NC pure Al and its alloys with GB segregation of Mg or Fe demonstrate the intergranular fracture leading to the samples failure. The main crack initiation and propagation mechanism is the formation of nano-voids along GBs followed by their growth and coalescence at higher stresses.

Overall, it was found that the GB segregation of Co has a positive effect on both ductility and strength of NC Al. The segregation of Fe can lead to NC Al strengthening but does not improve its ductility, and Ti demonstrates the opposite effect.

Deformation of NC Al is associated with the shear-coupled migration of GBs, i.e., with simultaneous GBS and GBM. GB segregation can significantly alter deformation mechanisms of NC Al promoting GBS and inhibiting GBM. Thus, the high strength of the NC Al with GB segregation of Co can be attributed to the ability of Co to detain both GBS and GBM.

Acknowledgements. Rita I. Babicheva thanks the Russian Science Foundation, grant No. 17-79-10410, for the financial support. Sergey V. Dmitriev and Vlarimir V. Stolyarov appreciate the financial support from the Russian Foundation for Basic Research, grant No. 16-58-48001.

References

1. R.Z. Valiev, R.K. Islamgaliev, I.V. Alexandrov. Progress in Materials Science 45 (2) (2000) 103 – 189.
2. A.P. Zhilyaev, T.G. Langdon. Progress in Materials Science 53 (6) (2008) 893 – 979.
3. R.Z. Valiev, T.G. Langdon. Progress in Materials Science 51 (7) (2006) 881 – 981.
4. R.Z. Valiev, A.V. Korznikov, R.R. Mulyukov. Materials Science and Engineering A168 (2) (1993) 141 – 148.
5. I. Sabirov, M.Y. Murashkin, R.Z. Valiev. Materials Science and Engineering A560 (2013) 1 – 24.
6. O. Sitdikov, E. Avtokratova, R. Babicheva, T. Sakai, K. Tsuzaki, Y. Watanabe. Materials Transactions 53 (01) (2012) 56 – 62.
7. R.I. Babicheva, K.A. Bukreeva, S.V. Dmitriev, K. Zhou. Computational Materials Science 79 (2013) 52 – 55.
8. R.I. Babicheva, K.A. Bukreeva, S.V. Dmitriev, R.R. Mulyukov, K. Zhou. Intermetallics 43 (2013) 171 – 176.
9. P. Lin, R.I. Babicheva, M. Xue, H.Sh. Zhang, H. Xu, B. Liu, K. Zhou. Computational Materials Science 96 (2015) 295 – 299.
10. K.A. Bukreeva, R.I. Babicheva, S.V. Dmitriev, K. Zhou, R.R. Mulyukov. Physics of the Solid State 55 (9) (2013) 1963 – 1967.
11. K.A. Bukreeva, R.I. Babicheva, A.B. Sultanguzhina, S.V. Dmitriev, K. Zhou, R.R. Mulyukov. Physics of the Solid State 56 (6) (2014) 1157 – 1162.
12. R.I. Babicheva, Kh.Ya. Mulyukov, I.Z. Sharipov, I.M. Safarov. Physics of the Solid State 54 (7) (2012) 1480 – 1485.
13. R.I. Babicheva, Kh.Ya. Mulyukov. Applied Physics A Materials Science & Processing 116 (4) (2014) 1857 – 1865
14. E.O. Hall. Proceedings of the Physical Society. Section B64 (1951) 747 – 753.
15. N.J. Petch, Journal of the Iron and Steel Institute. 174 (1953) 25 – 28.
16. M.F. Ashby, Philosophical Magazine 21 (1970), pp. 399 – 424.
17. J.C. M. Li and Y.T. Chou, Met. Mat. Trans. 1 (1970), pp. 1145 – 1159.
18. A. Sutton. Interfaces in crystalline materials. Oxford: Clarendon Press; New York: Oxford University Press (1995) xxxii, 819 p.
19. A.N. Chokshi, A. Rosen, J. Karch, H. Gleiter. Scr. Metall. 23 (1989) 1679.
20. D. Raabe, M. Herbig, S. Sandlöbes, Y. Li, D. Tytko, M. Kuzmina, D. Ponge, P.-P. Choi. Current Opinion in Solid State and Materials Science 18 (2014) 253 – 261.
21. R.Z. Valiev, N.A. Enikeev, M.Yu. Murashkin, V.U. Kazykhanov, X. Sauvage. Scripta Materialia 63 (9) (2010) 949 – 952.
22. Y. Nasedkina, X. Sauvage, E.V. Bobruk, M.Y. Murashkin,

R. Z. Valiev, N. A. Enikeev. J. Alloys and Compounds 710 (2017) 736.
23. M. M. Abramova, N. A. Enikeev, R. Z. Valiev, A. Etienne, B. Radiguet, Y. Ivanisenko, X. Sauvage. Materials Letters 136 (2014) 349.
24. X. Sauvage, N. Enikeev, R. Valiev, Y. Nasedkina, M. Murashkin. Acta Materialia 72 (2014) 125.
25. R. I. Babicheva, S. V. Dmitriev, Y. Zhang, S. W. Kok, N. Srikanth, B. Liu, K. Zhou. Computational Materials Science 98 (2015) 410 – 416.
26. R. Babicheva, D. Bachurin, S. Dmitriev, Y. Zhang, S. W. Kok, L. Bai, K. Zhou. Philosophical Magazine 96 (15) (2016) 1598 – 1612.
27. Y. J. Li, P. P. Choi, S. Goto, C. Borchers, D. Raabe, R. Kirchheim. Acta Materialia 60 (2012) 4005 – 4016.
28. R. Babicheva, S. Dmitriev, L. Bai, Y. Zhang, S. W. Kok, G. Kang, K. Zhou. Computational Materials Science 117 (2016) 445 – 454.
29. A. V. Zinovev, M. G. Bapanina, R. I. Babicheva, N. A. Enikeev, S. V. Dmitriev, K. Zhou. The Physics of Metals and Metallography 18 (1) (2017) 65 – 74.
30. S. J. Dillon, M. Tang, W. C. Carter, M. P. Harmer. Acta Materialia 55 (2007) 6208 – 6218.
31. Q. Gao, M. Widom. Current Opinion in Solid State and Materials Science 20 (5) (2016) 240 – 246.
32. O. Dmitrieva, D. Ponge, G. Inden, J. Millán, P. Choi, J. Sietsma, et al. Acta Materialia 59 (2011) 364 – 374.
33. D. Raabe, S. Sandlöbes, J. Millán, D. Ponge, H. Assadi, M. Herbig, et al. Acta Materialia 61 (2013) 6132 – 6152.
34. R. Babicheva, S. Dmitriev, D. Bachurin, N. Srikanth, Y. Zhang, S. W. Kok, K. Zhou. Int. J. Fatigue 102 (2017) 270 – 281.
35. M. S. Daw, M. I. Baskes. Physical Review B29 (12) (1984) 6443 – 6453.
36. M. I. Mendelev, M. J. Kramer, C. A. Becker, M. Asta. Philosophical Magazine 88 (12) (2008) 1723 – 1750.
37. M. I. Mendelev, M. Asta, M. J. Rahman, J. J. Hoyt. Philosophical Magazine 89 (2009) 3269 – 3285.
38. M. I. Mendelev, D. J. Srolovitz, G. J. Ackland, S. Han. Journal of Materials Research 20 (2005) 208 – 218.
39. R. R. Zope, Y. Mishin. Physical Review B68 (2003) 024102.
40. A. Landa, P. Wynblatt, D. J. Siegel, J. B. Adams, O. N. Mryasov, X.-Y. Liu. Acta Materialia 48 (2000) 1753 – 1761.
41. G. P. Purja Pun, V. Yamakov, Y. Mishin. Modelling and Simulation in Materials Science and Engineering 23 (2015) 065006.
42. S. Plimpton. Journal of Computational Physics 117 (1995) 1 – 19.
43. A. Stukowski. Modelling and Simulation in Materials Science and Engineering 18 (2010) 015012.
44. X. Zhou, X. Li, C. Chen. Acta Materialia 99 (2015) 77 – 86.
45. K. Nishimura, N. Miyazaki. Computational Materials Science 31 (2004) 269 – 278.
46. M. F. Horstemeyer, D. Farkas, S. Kim, T. Tang, G. Potirniche. International Journal of Fatigue 32 (2010) 1473 – 1502.
47. M. Legros, D. S. Gianola, K. J. Hemker. Acta Materialia 56 (2008) 3380 – 3393.
48. F. Mompiou, D. Caillard, M. Legros. Acta Materialia 57 (2009) 2198 – 2209.
49. I. A. Ovid'ko, A. G. Sheinerman, E. C. Aifantis. Acta Materialia 56 (2008) 2718 – 2727.
50. Y. Horio, A. Inoue, T. Masumoto. Materials Science and Engineering A179–180 (1994) 596 – 599.
51. R. I. Wu, G. Wilde, J. H. Perepezko. Materials Science and Engineering A301 (2001) 12–17.
52. E. G. Soboleva, A. L. Igisheva, T. B. Krit. IOP Conference Series: Materials Science and Engineering 91 (2015) 012032.